RSC Advances

PAPER

View Article Online
View Journal | View Issue

Check for updates

Cite this: *RSC Adv.*, 2019, **9**, 41913

Selective loading of platinum or silver cocatalyst onto a hydrogen-evolution photocatalyst in a silver-mediated all solid-state Z-scheme system for enhanced overall water splitting†

Junya Osaki,[a] Masaomi Yoda,[a] Toshihiro Takashima[ab] and Hiroshi Irie*[ab]

Received 12th November 2019
Accepted 11th December 2019

DOI: 10.1039/c9ra09421k

rsc.li/rsc-advances

We selectively loaded a hydrogen (H_2)-evolution cocatalyst, either platinum (Pt) or silver (Ag), onto a H_2-evolution photocatalyst, zinc rhodium oxide ($ZnRh_2O_4$), in a Ag-inserted $ZnRh_2O_4$ and bismuth vanadium oxide ($Bi_4V_2O_{11}$) hetero-junction photocatalyst ($ZnRh_2O_4/Ag/Bi_4V_2O_{11}$) by a photo-deposition method. The selective loading of Pt or Ag was achieved by taking advantage of the band-gap difference between $ZnRh_2O_4$ (1.2 eV) and $Bi_4V_2O_{11}$ (1.7 eV) and increased the overall water-splitting activity of the photocatalyst.

Hydrogen (H_2) is a versatile, non-polluting energy carrier because the chemical energy stored in the H–H bond is released when H_2 combines with oxygen (O_2) and yields only water as the reaction product. Accordingly, an energy infrastructure based on H_2 represents an ideal solution to energy-related environmental issues for reducing carbon dioxide (CO_2) emissions. Photocatalytic water-splitting using sunlight represents one of the cleanest methods to produce H_2.[1] Since the Honda–Fujishima effect was first reported in 1972,[2] various water-splitting methods, including electrode and powder systems, have been extensively investigated for the possibility of simple, large scale production of H_2.[2,3] Following the demonstration by Domen and coworkers that a solid solution of gallium nitride (GaN)–zinc oxide (ZnO) is capable of splitting water at wavelengths up to ~480 nm,[4] numerous researchers have attempted to identify powdered photocatalysts that utilize longer wavelengths of visible light for efficient water-splitting using solar energy.[5]

Previously, we fabricated a hetero-junction photocatalyst consisting of zinc rhodium oxide ($ZnRh_2O_4$) and bismuth vanadium oxide ($Bi_4V_2O_{11}$), which functioned as H_2- and O_2-evolution photocatalysts, respectively, and either silver (Ag) or gold (Au) as a conductive layer ($ZnRh_2O_4/Ag/Bi_4V_2O_{11}$ or $ZnRh_2O_4/Au/Bi_4V_2O_{11}$) after Tada and coworkers.[6] Recently, similar hetero-junction photocatalysts were reported.[7]

In $ZnRh_2O_4/Ag/Bi_4V_2O_{11}$ or $ZnRh_2O_4/Au/Bi_4V_2O_{11}$, overall pure water-splitting proceeded under irradiation with red light (wavelengths larger than 700 nm)[8–10] *via* Ag or Au, which mediated the transfer of photo-excited electrons from the conduction band (CB) of $Bi_4V_2O_{11}$ to the valence band (VB) of $ZnRh_2O_4$. Thus, the photo-excited electrons in $ZnRh_2O_4$ and holes in $Bi_4V_2O_{11}$ effectively reduced and oxidized water, respectively, to accomplish overall water splitting. The modification of the cocatalyst with a metal or metal oxide is essential to enhance the water-splitting activity. The selective loading of a H_2-favorable cocatalyst onto $ZnRh_2O_4$ is expected to increase H_2 evolution and thereby increase the overall water-splitting activity of this hetero-junction photocatalyst. Here, we used platinum (Pt) and Ag as H_2-evolution cocatalysts and attempted to selectively deposit Pt or Ag onto $ZnRh_2O_4$ in $ZnRh_2O_4/Ag/Bi_4V_2O_{11}$.

Powdered $ZnRh_2O_4/Ag/Bi_4V_2O_{11}$ (molar ratio of $ZnRh_2O_4$ to $Bi_4V_2O_{11}$ was 1.0 : 1.2) was prepared following procedures previously reported procedures (ESI-1†)[8] and the photo-deposition of Pt or Ag was conducted under light irradiation at wavelength longer than 850 nm. Under these irradiation conditions, only $ZnRh_2O_4$ was photo-excited because the energy of irradiated light was higher than band-gap energy of $ZnRh_2O_4$ (1.2 eV) but smaller than that of $Bi_4V_2O_{11}$ (1.7 eV). Due to the specific photoexcitation of $ZnRh_2O_4$, Pt or Ag was only photo-deposited onto this material, generating $Pt/ZnRh_2O_4/Ag/Bi_4V_2O_{11}$ and $Ag/ZnRh_2O_4/Ag/Bi_4V_2O_{11}$ (ESI-1†).

In the powder XRD pattern of $ZnRh_2O_4/Ag/Bi_4V_2O_{11}$ (Fig. S1, ESI-2†), the observed peaks mainly corresponded to two phases originating from $ZnRh_2O_4$ and $Bi_4V_2O_{11}$, with the trace peaks ascribed to an unknown Ag oxide (likely $AgVO_3$). Notably, no Ag peaks were observed in the XRD spectrum, which is plausible since the amount of Ag remaining in the composite was too small for detection. These observations are consistent with those reported previously.[8] The valency of Ag in the

[a]*Special Doctoral Program for Green Energy Conversion Science and Technology, Integrated Graduate School of Medicine, Engineering, and Agricultural Sciences, University of Yamanashi, 4-3-11 Takeda, Kofu, Yamanashi 400-8511, Japan*

[b]*Clean Energy Research Center, University of Yamanashi, 4-3-11 Takeda, Kofu, Yamanashi 400-8511, Japan. E-mail: hirie@yamanashi.ac.jp*

† Electronic supplementary information (ESI) available. See DOI: 10.1039/c9ra09421k

photocatalyst was determined by XPS to be mainly zero (Ag^0). The implications of this finding are discussed below.

UV-vis absorption spectra of $ZnRh_2O_4/Ag/Bi_4V_2O_{11}$, $Pt/ZnRh_2O_4/Ag/Bi_4V_2O_{11}$, and $Ag/ZnRh_2O_4/Ag/Bi_4V_2O_{11}$ are shown in Fig. 1. In the spectra, $Pt/ZnRh_2O_4/Ag/Bi_4V_2O_{11}$ and $Ag/ZnRh_2O_4/Ag/Bi_4V_2O_{11}$ had greater absorption than that of $ZnRh_2O_4/Ag/Bi_4V_2O_{11}$ in the longer wavelength region, a property that is derived from the deposited Pt and Ag.

Fig. 2a–f show XPS spectra of $ZnRh_2O_4/Ag/Bi_4V_2O_{11}$, $Pt/ZnRh_2O_4/Ag/Bi_4V_2O_{11}$, and $Ag/ZnRh_2O_4/Ag/Bi_4V_2O_{11}$ for Bi 4f (Fig. 2a), V 2p (Fig. 2b), Zn 2p (Fig. 2c), Rh 3d (Fig. 2d), Ag 3d (Fig. 2e), and Pt 4f (Fig. 2f). As we assumed that the cocatalyst, Pt or Ag, was selectively deposited onto $ZnRh_2O_4$ and the $Bi_4V_2O_{11}$ surface remained unaltered after the deposition of the cocatalyst, all of the XPS peaks were normalized using the peak areas of Bi 4f for the bare, Pt-deposited, and Ag-deposited $ZnRh_2O_4/Ag/Bi_4V_2O_{11}$ photocatalysts (Fig. 2a). It was reasonable that the peak areas in the normalized V $2p_{3/2}$ spectra of the three photocatalysts were similar (Fig. 2b). Further, the normalized Zn 2p and Rh 3d peaks of $Pt/ZnRh_2O_4/Ag/Bi_4V_2O_{11}$ and $Ag/ZnRh_2O_4/Ag/Bi_4V_2O_{11}$ were smaller than those of $ZnRh_2O_4/Ag/Bi_4V_2O_{11}$ (Fig. 2c and d). The results of the surface-sensitive XPS measurements indicate that Pt and Ag were selectively deposited onto $ZnRh_2O_4$.

The normalized Ag 3d peak area of $Pt/ZnRh_2O_4/Ag/Bi_4V_2O_{11}$ was quite similar to that of $ZnRh_2O_4/Ag/Bi_4V_2O_{11}$ (Fig. 2e). This result is reasonable because the Ag 3d spectra of the two photocatalysts are attributable to the Ag inserted between $ZnRh_2O_4$ and $Bi_4V_2O_{11}$. In contrast, the Ag 3d spectrum of $Ag/ZnRh_2O_4/Ag/Bi_4V_2O_{11}$ was larger than those of $Pt/ZnRh_2O_4/Ag/Bi_4V_2O_{11}$ and $ZnRh_2O_4/Ag/Bi_4V_2O_{11}$, indicating that the former spectrum originated from the photo-deposited Ag and Ag located between $ZnRh_2O_4$ and $Bi_4V_2O_{11}$. In the normalized Pt 4f spectra, the Pt 4f peaks were only observed on $Pt/ZnRh_2O_4/Ag/Bi_4V_2O_{11}$ and were not detected in the XPS spectra of $Ag/ZnRh_2O_4/Ag/Bi_4V_2O_{11}$ and $ZnRh_2O_4/Ag/Bi_4V_2O_{11}$ (Fig. 2f).

To quantitatively analyze the amounts and determine the valencies of Pt and Ag in the three photocatalysts, a peak deconvolution method was applied to the Bi 4f, Ag 3d, and Pt 4f spectra (Fig. S2 in ESI-3†). As we considered that the $Bi_4V_2O_{11}$ surface remained unaltered after the Pt or Ag deposition, we estimated the amount of Pt or Ag in the photocatalysts based on the amount of Bi. First, peak deconvolution for Bi 4f was performed with the following parameters. The binding energies of Bi $4f_{7/2}$ and Bi $4f_{5/2}$ of Bi^{3+} were fixed at 159.5 ± 0.1 eV and 164.8 ± 0.1 eV, respectively.[11] For the Pt- and Ag-deposited photocatalysts, an additional pair of small peaks was observed at 161.0 ± 0.1 eV and 166.3 ± 0.1 eV. The origin of the additional peaks was unclear; however, the peaks were likely derived from Bi^{3+}–Cl^- (*e.g.*, BiOCl)[12] or Bi^{3+}–NO_3^- ($Bi(NO_3)_3$) remaining on the surface because Pt or Ag was photo-deposited in the $H_2PtCl_6\cdot 6H_2O$ or $AgNO_3$ solution despite thorough washing with distilled water. The peak area ratio of Bi $4f_{5/2}$ to Bi $4f_{7/2}$ for Bi^{3+} was fixed at 0.75 (Fig. S2a, S2c, S2f and Table S1 in ESI-3†).

In Fig. S2b, S2d, and S2g in ESI-3,† the Ag 3d peaks for the three photocatalysts were deconvoluted by a pair of Ag 3d peaks (Ag $3d_{5/2}$ and Ag $3d_{3/2}$, with binding energies of 368.6 ± 0.1 eV and 374.6 ± 0.1 eV, respectively), which is attributable to metallic Ag (Ag^0).[8,9,13] These results indicate that Ag was inserted as a metallic particle between $ZnRh_2O_4$ and $Bi_4V_2O_{11}$ in $ZnRh_2O_4/Ag/Bi_4V_2O_{11}$, $Pt/ZnRh_2O_4/Ag/Bi_4V_2O_{11}$, and $Ag/ZnRh_2O_4/Ag/Bi_4V_2O_{11}$.[8,9] In addition, the Ag cocatalyst was also proved to be deposited as the metallic one. In contrast, the Pt 4f

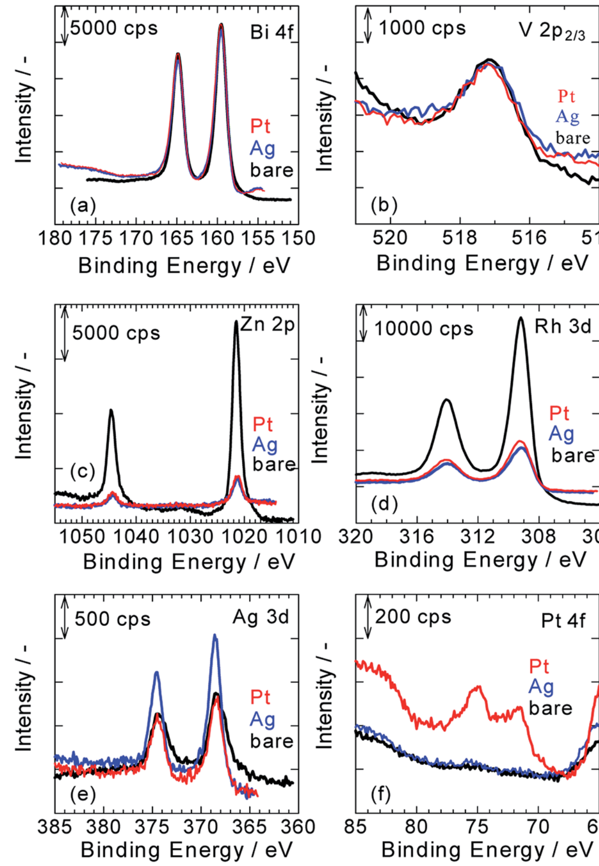

Fig. 2 Normalized XPS spectra of $ZnRh_2O_4/Ag/Bi_4V_2O_{11}$ (black lines), $Pt/ZnRh_2O_4/Ag/Bi_4V_2O_{11}$ (red lines), and $Ag/ZnRh_2O_4/Ag/Bi_4V_2O_{11}$ (blue lines) for Bi 4f (a), V 2p (b), Zn 2p (c), Rh 3d (d), Ag 3d (e), and Pt 4f (f). All spectra were calibrated with the C 1s peak, which was derived from a surface-contaminant hydrocarbon with a binding energy of 284.5 eV.

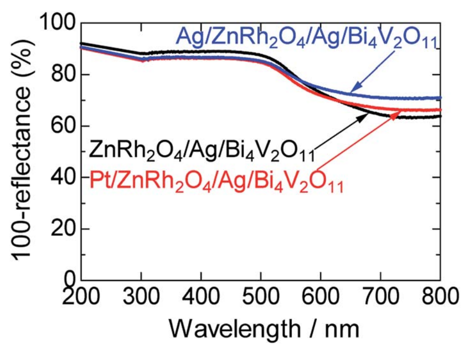

Fig. 1 UV-visible absorption spectra of $ZnRh_2O_4/Ag/Bi_4V_2O_{11}$, $Pt/ZnRh_2O_4/Ag/Bi_4V_2O_{11}$, and $Ag/ZnRh_2O_4/Ag/Bi_4V_2O_{11}$.

peaks for $Pt/ZnRh_2O_4/Ag/Bi_4V_2O_{11}$ were deconvoluted by three pairs of Pt 4f peaks with binding energies of 71.3 eV (Pt $4f_{7/2}$) and 74.6 eV (Pt $4f_{5/2}$) for metallic Pt (Pt^0), 72.3 eV (Pt $4f_{7/2}$) and 75.6 eV (Pt $4f_{5/2}$) for Pt^{2+}, and 73.3 eV (Pt $4f_{7/2}$) and 76.6 eV (Pt $4f_{5/2}$) for Pt^{3+} (Fig. S2e in ESI-3†).[14] The total Pt^0, Pt^{2+}, and Pt^{3+} areas were determined by summing the corresponding deconvolution areas of Pt $4f_{5/2}$ and Pt $4f_{7/2}$ (Table S1 in ESI-3†). The atomic ratios of Pt^0, Pt^{2+}, and Pt^{3+} *vs.* total Pt were calculated to be 0.63, 0.25, and 0.12, respectively, and by dividing the total Pt^0, Pt^{2+}, and Pt^{3+} areas by the total Pt area and represent the sum of the total Pt^0, Pt^{2+}, and Pt^{3+} areas. Thus, the major Pt species that functioned as the cocatalyst was Pt^0; however, Pt^{4+} was not fully reduced to Pt^0. The valence distribution was not observed for Ag, but observed for Pt. We are considering two possible explanations; one is a difference in the reduction potential between Ag and Pt deposition, $Ag^+ + e^- \rightarrow Ag^0$ (0.80 V *vs.* SHE), $PtCl_6{}^{2-} + 2e^- \rightarrow PtCl_4{}^{2-} + 2Cl^-$ ($Pt^{4+} \rightarrow Pt^{2+}$, 0.68 V *vs.* SHE), $PtCl_4{}^{2-} + 2e^- \rightarrow Pt^0 + 4Cl^-$ ($Pt^{2+} \rightarrow Pt^0$, 0.72 V *vs.* SHE) although that of $PtCl_6{}^{2-} + e^- \rightarrow PtCl_5{}^{2-} + Cl^-$ is unknown. Thus, forming Ag^0 from the reduction of Ag^+ is thermodynamically more favorable than forming Pt^{2+} from that of Pt^{4+} and Pt^0 from that of Pt^{2+}. The other reason is that the reduction product from Ag^+ is only Ag^0, but some reduction products are possible from Pt^{4+}, such as Pt^{3+}, Pt^{2+}, Pt^+, and Pt^0, if the reduction proceeds. In fact, Pt^{4+} was not detected, and the reduction of Pt^{4+} proceeded.

The Ag and Bi areas were determined by summing the deconvolution areas of Ag $3d_{5/2}$ and Ag $3d_{3/2}$, and those of Bi $4f_{7/2}$ and Bi $4f_{5/2}$, respectively (Table S1 in ESI-3†). The atomic ratio of Ag to Bi was then calculated based on the Ag 3d (5.99) and Bi 4f sensitivity factors (9.14),[15] and the mole percent of Ag to that of the sum of $ZnRh_2O_4$ and $Bi_4V_2O_{11}$ (1.0 mole of $ZnRh_2O_4$ + 1.2 mole of $Bi_4V_2O_{11}$) was determined. The weight percent (wt%) of Ag in the three photocatalysts was recalculated (Table S2 in ESI-3†). As expected, the amount of Ag in $ZnRh_2O_4/Ag/Bi_4V_2O_{11}$ and $Pt/ZnRh_2O_4/Ag/Bi_4V_2O_{11}$ was identical at 2.1 wt%. Thus, the Ag cocatalyst deposited in $Ag/ZnRh_2O_4/Ag/Bi_4V_2O_{11}$ was estimated to be 1.1 wt% based on the assumption that the amount of Ag inserted in $Ag/ZnRh_2O_4/Ag/Bi_4V_2O_{11}$ was 2.1 wt%. Similarly, the amount of Pt cocatalyst in $Pt/ZnRh_2O_4/Ag/Bi_4V_2O_{11}$ was calculated to be 1.2 wt% (Table S2† in ESI-3†) based on the total Pt area and Pt 4f sensitivity factor (5.575).[15]

SEM images of $ZnRh_2O_4/Ag/Bi_4V_2O_{11}$, $Pt/ZnRh_2O_4/Ag/Bi_4V_2O_{11}$, and $Ag/ZnRh_2O_4/Ag/Bi_4V_2O_{11}$ powders are shown (Figs. S3a–c in ESI-4†). All images were quite similar, and small $ZnRh_2O_4$ (∼200 nm) and large $Bi_4V_2O_{11}$ (∼10 μm) particles can be clearly observed. However, the photo-deposited Pt and Ag were not observed.

STEM imaging (high angle annular dark-field (HAADF), bright-field (BF)) and EDS-based elemental mapping of $Pt/ZnRh_2O_4/Ag/Bi_4V_2O_{11}$ were performed (Fig. 3a–g). In the HAADF-STEM image (Fig. 3a), $ZnRh_2O_4$ and $Bi_4V_2O_{11}$ particles were clearly distinguishable based on the SEM image (Fig. S3b in ESI-4†) and their previously reported sizes of ∼200 nm and ∼10 μm, respectively.[8] Thus, the small aggregated particles in the HAADF-STEM image were $ZnRh_2O_4$ and were adjacent to a large particle of $Bi_4V_2O_{11}$. The particle compositions were confirmed by the EDS-based elemental mapping of Bi and Rh in Fig. 3c and e, respectively. In addition, Ag particles were detected (Fig. 3d) between the areas of Bi (Fig. 3c) and Rh (Fig. 3e), indicating that Ag was inserted between the $ZnRh_2O_4$ and $Bi_4V_2O_{11}$ particles. This finding was also confirmed by the line elemental analysis (Fig. 3g). Notably, the atomic percentages of Bi and V decreased at the boundary of Ag and $ZnRh_2O_4$, and those of Zn and Rh increased at the boundary of Ag and $Bi_4V_2O_{11}$. Accordingly, the percentage of Ag increased and

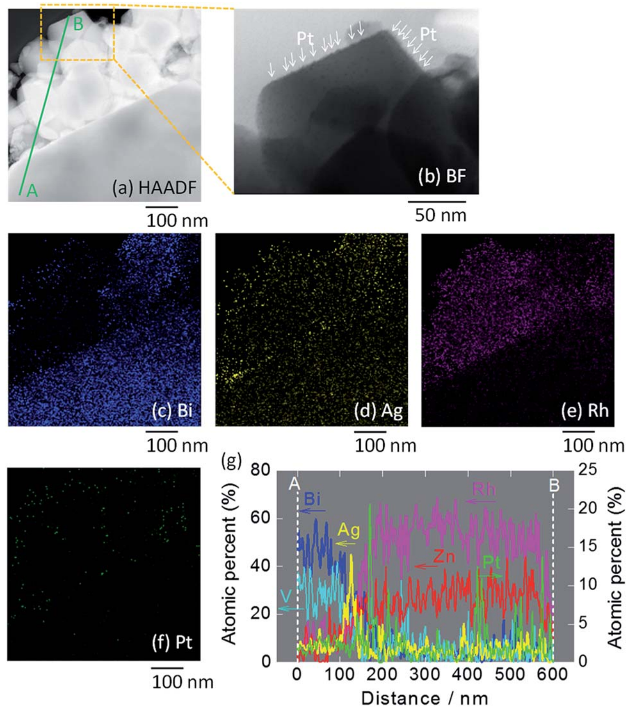

Fig. 3 STEM images of $Pt/ZnRh_2O_4/Ag/Bi_4V_2O_{11}$. HAADF-STEM image (a) and the BF enlargement (b) in which Pt is indicated by arrows, and EDS elemental maps (c–f), in which blue (c), yellow (d), pink (e), and green (f) colors correspond to Bi, Ag, Rh, and Pt, respectively. In (a), the line along which the elemental analysis was performed is shown (A to B). Atomic percentages of Bi, V, Zn, Rh, Ag, and Pt measured from the area of $Bi_4V_2O_{11}$ (A) to that of $ZnRh_2O_4$ (B) (g). Enlarged images of (a)–(f) are shown in ESI-5.†

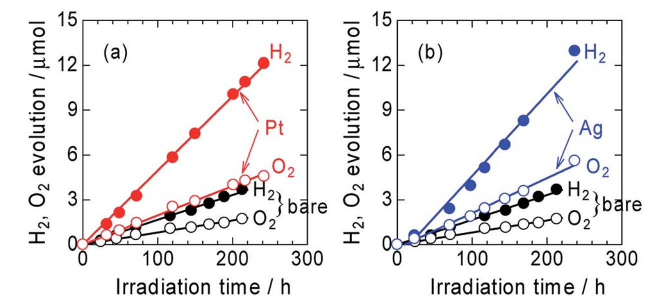

Fig. 4 Time courses of photocatalytic evolution of H_2 and O_2 from water over $Pt/ZnRh_2O_4/Ag/Bi_4V_2O_{11}$ (a) and $Ag/ZnRh_2O_4/Ag/Bi_4V_2O_{11}$ (b) irradiated with 700 nm LED light. For comparison, the evolution of H_2 and O_2 over bare $ZnRh_2O_4/Ag/Bi_4V_2O_{11}$ is also shown.

Table 1 Light intensity, H_2 generation rates, and AQE values in the presence of $ZnRh_2O_4/Ag/Bi_4V_2O_{11}$, $Pt/ZnRh_2O_4/Ag/Bi_4V_2O_{11}$ and $Ag/ZnRh_2O_4/Ag/Bi_4V_2O_{11}$

Light source	Light/mW cm^{-2}	H_2 evolution rate/μmol h^{-1}	AQE/%
$ZnRh_2O_4/Ag/Bi_4V_2O_{11}$	2.9	1.7×10^{-2}	1.5×10^{-2}
$Pt/ZnRh_2O_4/Ag/Bi_4V_2O_{11}$	3.5	5.0×10^{-2}	4.1×10^{-2}
$Ag/ZnRh_2O_4/Ag/Bi_4V_2O_{11}$	3.5	5.5×10^{-2}	4.6×10^{-2}

decreased at the boundary with $Bi_4V_2O_{11}$ and $ZnRh_2O_4$, respectively, indicating that Ag was present at the $Bi_4V_2O_{11}$ and $ZnRh_2O_4$ interface. As expected, Pt was only deposited onto $ZnRh_2O_4$ because Pt was only distributed in the vicinity of Rh (Fig. 3f). This finding was also confirmed by the line elemental analysis, as several sharp peaks derived from Pt were observed in the area of $ZnRh_2O_4$ (Fig. 3g). In addition, extremely small particles, corresponding to Pt, were observed only on $ZnRh_2O_4$ in the enlarged BF image of $Pt/ZnRh_2O_4/Ag/Bi_4V_2O_{11}$ (Fig. 3b).

The time courses of H_2 and O_2 evolution from $Pt/ZnRh_2O_4/Ag/Bi_4V_2O_{11}$ and $Ag/ZnRh_2O_4/Ag/Bi_4V_2O_{11}$ in comparison with $ZnRh_2O_4/Ag/Bi_4V_2O_{11}$ under monochromic light irradiation at a wavelength of 700 nm were measured (Fig. 4a and b). The three photocatalysts evolved H_2 and O_2 from water at a molar ratio of ~2 to 1 (2.1 to 1, 2.3 to 1, and 2.2 to 1 for $ZnRh_2O_4/Ag/Bi_4V_2O_{11}$, $Pt/ZnRh_2O_4/Ag/Bi_4V_2O_{11}$, and $Ag/ZnRh_2O_4/Ag/Bi_4V_2O_{11}$, respectively), indicating that the overall water-splitting reaction proceeded efficiently. The band alignments of $ZnRh_2O_4$, Ag, and $Bi_4V_2O_{11}$, and the charge transfer process are shown in Scheme S1 (ESI-6†). The photo-excited electrons in $ZnRh_2O_4$ and holes in $Bi_4V_2O_{11}$ can effectively reduce and oxidize water, respectively. Specifically, Ag acted as a solid-state electron mediator for the electron transfer from the CB of $Bi_4V_2O_{11}$ to the VB of $ZnRh_2O_4$. The deposition of Pt or Ag enhanced the H_2 and O_2 evolution rates, demonstrating that Pt and Ag functioned as cocatalysts for the overall water-splitting reaction. The apparent quantum efficiency (AQE) values for the reaction over $Pt/ZnRh_2O_4/Ag/Bi_4V_2O_{11}$ (4.1×10^{-2}%) and $Ag/ZnRh_2O_4/Ag/Bi_4V_2O_{11}$ (4.6×10^{-2}%) were ~3-fold higher than that over $ZnRh_2O_4/Ag/Bi_4V_2O_{11}$ (1.5×10^{-2}%) (Tables 1 and S3 in ESI-7†).

We previously reported that the treatment of $ZnRh_2O_4/Ag/Bi_4V_2O_{11}$ with nitric acid (HNO_3) is required to achieve overall water splitting (ESI-1†). The treatment removes excess Ag containing Ag^+ which is a sacrificial agent for O_2 evolution.[8,9] Thus, without HNO_3 treatment, excess Ag remaining on $Bi_4V_2O_{11}$ in $ZnRh_2O_4/Ag/Bi_4V_2O_{11}$ evolves O_2 even from water, resulting in more O_2 being released than that of the stoichiometric amount of O_2 to H_2 of ~1 to 2. However, in the present study, H_2 and O_2 were evolved at a 2 : 1 ratio, providing further evidence that Ag was selectively deposited onto $ZnRh_2O_4$. Notably, Ag-deposited $ZnRh_2O_4$ is unable to evolve O_2 from water because the VB top potential of $ZnRh_2O_4$ lies at ~0.1 V (*vs.* SHE, pH = 0),[16] which is thermodynamically unfavorable for O_2 evolution.

In conclusion, Pt or Ag as a cocatalyst was selectively photodeposited onto $ZnRh_2O_4$ in $ZnRh_2O_4/Ag/Bi_4V_2O_{11}$ and resulted in the enhancement of stoichiometric H_2 and O_2 evolution from water. $ZnRh_2O_4/Ag/Bi_4V_2O_{11}$ also has the potential to reduce CO_2 under visible-light irradiation to carbon monoxide (CO), formate, methanol, methane, and other hydrocarbons using water as an electron source. Notably, when present on $ZnRh_2O_4$, Ag acts as a selective cocatalyst for the conversion of CO_2 to CO. In contrast, as Pt lacks this property, different reaction products can be detected. Such studies are currently underway in our laboratory.

Conflicts of interest

There are no conflicts to declare.

Acknowledgements

This work was supported by JSPS KAKENHI (Grant-in-Aid for Scientific Research) (B), Grant Number 17H03126. We express gratitude to Mr G. Newton for the careful reading of the manuscript.

Notes and references

1 R. M. Navarro, M. A. Pena and J. L. G. Fierro, *Chem. Rev.*, 2007, **107**, 3952–3991.
2 A. Fujishima and K. Honda, *Nature*, 1972, **238**, 37–38.
3 O. Khaselev and J. A. Turner, *Science*, 1998, **280**, 425–427; W. J. Youngblood, S.-H. A. Lee, Y. Kobayashi, E. A. Hernandez-Pagan, P. G. Hoertz, T. A. Moore, A. L. Moore, D. Gust and T. E. Mallouk, *J. Am. Chem. Soc.*, 2009, **131**, 926–927; S. Y. Reece, J. A. Hamel, K. Sung, T. D. Jarvi, A. J. Esswein, J. J. H. Pijpers and D. G. Nocera, *Science*, 2011, **334**, 645–648; M. R. Singh, K. Papadantonakis, C. Xiang and N. S. Lewis, *Energy Environ. Sci.*, 2015, **8**, 2760–2767; S. Haussener, C. Xiang, J. M. Spurgeon, S. Ardo, N. S. Lewis and A. Z. Weber, *Energy Environ. Sci.*, 2012, **5**, 9922–9935; M. R. Singh, C. Xiang and N. S. Lewis, *Sustainable Energy Fuels*, 2017, **1**, 458–466; M. G. Walter, E. L. Warren, J. R. McKone, S. W. Boettcher, Q. Mi, E. A. Santori and N. S. Lewis, *Chem. Rev.*, 2010, **110**, 6446–6473; T. R. Cook, D. K. Dogutan, S. Y. Reece, Y. Surendranath, T. S. Teets and D. G. Nocera, *Chem. Rev.*, 2010, **110**, 6474–6502; K. Maeda and K. Domen, *J. Phys. Chem. Lett.*, 2010, **1**, 2655–2661.
4 K. Maeda, K. Teramura, D. Lu, T. Takata, N. Saito, Y. Inoue and K. Domen, *Nature*, 2006, **440**, 295.
5 L. Liao, Q. Zhang, Z. Su, Z. Zhao, Y. Wang, Y. Li, X. Lu, D. Wei, G. Feng, Q. Yu, *et al.*, *Nat. Nanotechnol.*, 2014, **9**,

69–73; C. Pan, T. Takata, M. Nakabayashi, T. Matsumoto, N. Shibata, Y. Ikuhara and K. Domen, *Angew. Chem., Int. Ed.*, 2015, **54**, 2955–2959; J. Liu, Y. Liu, N. Liu, Y. Han, X. Zhang, H. Huang, Y. Lifshitz, S. T. Lee, J. Zhong and Z. Kang, *Science*, 2015, **347**, 970–974.

6 H. Tada, T. Mitsui, T. Kiyonaga, T. Akita and K. Tanaka, *Nat. Mater.*, 2006, **5**, 782–786.

7 Y. Sasaki, H. Nemoto, K. Saito and A. Kudo, *J. Phys. Chem. C*, 2009, **113**, 17536–17542; A. Iwase, Y. H. Ng, Y. Ishiguro, A. Kudo and R. Amal, *J. Am. Chem. Soc.*, 2011, **133**, 11054–11057; Z. Pan, T. Hisatomi, Q. Wang, S. Chen, M. Nakabayashi, N. Shibata, C. Pan, T. Takata, M. Katayama, T. Minegishi, A. Kudo and K. Domen, *ACS Catal.*, 2016, **6**, 7188–7196; Q. Wang, T. Hisatomi, Q. Jia, H. Tokudome, M. Zhong, C. Wang, Z. Pan, T. Takata, M. Nakabayashi, N. Shibata, Y. Li, I. D. Sharp, A. Kudo, T. Yamada and K. Domen, *Nat. Mater.*, 2016, **15**, 611–615; S. Sun, T. Hisatomi, Q. Wang, S. Chen, G. Ma, J. Liu, S. Nandy, T. Minegishi, M. Katayama and K. Domen, *ACS Catal.*, 2018, **8**, 1690–1696.

8 R. Kobayashi, K. Kurihara, T. Takashima, B. Ohtani and H. Irie, *J. Mater. Chem. A*, 2016, **4**, 3061–3067.

9 R. Kobayashi, T. Takashima, S. Tanigawa, S. Takeuchi, B. Ohtani and H. Irie, *Phys. Chem. Chem. Phys.*, 2016, **18**, 27693–28378.

10 K. Kamijyo, T. Takashima, M. Yoda, J. Osaki and H. Irie, *Chem. Commun.*, 2018, **54**, 7999–8002.

11 Q. Jia, K. Iwashima and A. Kudo, *Proc. Natl. Acad. Sci. U. S. A.*, 2012, **109**, 11564–11569.

12 L. Ye, K. Deng, F. Xe, L. Tian, T. Peng and L. Zan, *Phys. Chem. Chem. Phys.*, 2012, **14**, 82–85.

13 G. B. Houflund, Z. F. Hazos and G. N. Salaita, *Phys. Rev. B: Condens. Matter Mater. Phys.*, 2000, **62**, 4482–4486; K. Kuribayashi and S. Kitamura, *Thin Solid Films*, 2001, **400**, 160–164.

14 Y. Abe, H. Yanagizawa and K. Sasaki, *Jpn. J. Appl. Phys.*, 1998, **37**, 11126–11133.

15 A. J. Bard, R. Parsons and J. Jordan, *Standard Potentials in Aqueous Solution*, 1985, New York, Marcel Dekker.

16 Y. Takimoto, T. Kitta and H. Irie, *Int. J. Hydrogen Energy*, 2012, **37**, 134–138.